

Investigation of Primordial Black Hole Bursts using Interplanetary Network Gamma-ray Bursts

T. N. Ukwatta

*Director's Postdoctoral Fellow, Space and Remote Sensing (ISR-2), Los Alamos National
Laboratory, Los Alamos, NM 87545, USA.*

tilan@lanl.gov

K. Hurley

*University of California, Berkeley, Space Sciences Laboratory, 7 Gauss Way, Berkeley, CA
94720-7450, USA*

J. H. MacGibbon

Department of Physics, University of North Florida, Jacksonville, FL 32224, USA

the following authors are in order of the number of times their experiments were used in the paper

D. S. Svinkin, R. L. Aptekar, S. V. Golenetskii, D. D. Frederiks, V. D. Pal'shin

Ioffe Physical Technical Institute, St. Petersburg, 194021, Russian Federation

J. Goldsten

Applied Physics Laboratory, Johns Hopkins University, Laurel, MD 20723, U.S.A.

W. Boynton

University of Arizona, Department of Planetary Sciences, Tucson, Arizona 85721, U.S.A.

A. S. Kozyrev

Space Research Institute, 84/32, Profsoyuznaya, Moscow 117997, Russian Federation

A. Rau, A. von Kienlin, X. Zhang

*Max-Planck-Institut für extraterrestrische Physik, Giessenbachstrasse, Postfach 1312, Garching,
85748 Germany*

V. Connaughton

University of Alabama in Huntsville, NSSTC, 320 Sparkman Drive, Huntsville, AL 35805, USA

K. Yamaoka

*Department of Physics and Mathematics, Aoyama Gakuin University, 5-10-1 Fuchinobe,
Sagamihara, Kanagawa 229-8558, Japan*

M. Ohno

*Department of Physics, Hiroshima University, 1-3-1 Kagamiyama, Higashi-Hiroshima, Hiroshima
739-8526, Japan*

N. Ohmori

*Department of Applied Physics, University of Miyazaki, 1-1 Gakuen kibanadai-nishi,
Miyazaki-shi, Miyazaki 889-2192, Japan*

M. Feroci

INAF/IAPS-Roma, via Fosso del Cavaliere 100, 00133, Roma, Italy

F. Frontera¹, C. Guidorzi

University of Ferrara, Dept. of Physics and Earth Science, via Saragat 1, 44122 Ferrara, Italy

T. Cline², N. Gehrels

NASA Goddard Space Flight Center, Code 661, Greenbelt, MD 20771, U.S.A.

H. A. Krimm⁴

USRA/CRESST/NASA Goddard Space Flight Center, Code 661, Greenbelt, MD 20771, U.S.A.

J. McTiernan

*University of California, Berkeley, Space Sciences Laboratory, 7 Gauss Way, Berkeley, CA
94720-7450, USA*

ABSTRACT

The detection of a gamma-ray burst (GRB) in the solar neighborhood would have very important implications for GRB phenomenology. The leading theories for cosmological GRBs would not be able to explain such events. The final bursts of evaporating

¹INAF/Istituto di Astrofisica Spaziale e Fisica Cosmica di Bologna, via Gobetti 101, I-40129 Bologna, Italy

²Emeritus

³Joint Center for Astrophysics, University of Maryland, Baltimore County, 1000 Hilltop Circle, Baltimore, MD 21250

⁴Universities Space Research Association, 10211 Wincopin Circle, Suite 500, Columbia, MD 21044

Primordial Black Holes (PBHs), however, would be a natural explanation for local GRBs. We present a novel technique that can constrain the distance to gamma-ray bursts using detections from widely separated, non-imaging spacecraft. This method can determine the actual distance to the burst if it is local. We applied this method to constrain distances to a sample of 36 short duration GRBs detected by the Interplanetary Network (IPN) that show observational properties that are expected from PBH evaporations. These bursts have minimum possible distances in the 10^{13} – 10^{18} cm (7 – 10^5 AU) range, consistent with the expected PBH energetics and with a possible origin in the solar neighborhood, although none of the bursts can be unambiguously demonstrated to be local. Assuming these bursts are real PBH events, we estimate lower limits on the PBH burst evaporation rate in the solar neighborhood.

Subject headings: primordial black holes; black hole physics; gamma-ray bursts: general

1. Introduction

The composition of the short-duration, hard-spectrum gamma-ray burst (GRB) population is not yet fully understood. It is believed that most of the bursts are generated in compact binary mergers (Eichler et al. 1989) and while the handful of optical counterparts and host galaxies discovered to date does not contradict this view, it is also thought that the population probably contains up to 8% extragalactic giant magnetar flares as well (Hurley et al. 2010; Mazets et al. 2008; Svinkin et al. 2015a). For the majority of the short-duration GRB population, however, there is simply not enough evidence to determine their origin unambiguously. Hawking radiation from primordial black holes (hereafter PBH) was one of the very first explanations proposed for cosmic gamma-ray bursts (Hawking 1974), and it continues to be proposed today (Cline and Hong 1996; Czerny et al. 1996; Cline et al. 1997, 1999, 2003, 2005; Czerny et al. 2011). The PBH lifetime and burst duration depend on its mass, so PBHs bursting today have similar masses and durations, and release similar energies, making them in essence ‘standard candles’. The typical PBH gamma-ray burst is not expected to be accompanied by detectable intrinsically-generated extended emission or have an afterglow, although accompanying bursts at other wavelengths or afterglows may arise if, for example, the PBH is embedded in a high density magnetic field or plasma (MacGibbon et al. 2008; Rees 1977; Jelley, Baird, and O’Mongain 1977). In the standard emission scenario, so-called because it uses the Standard Model of particle physics (MacGibbon and Webber 1990), the PBH gamma-ray burst is strongest in the final second of the burst lifetime, has a hard energy spectrum, and should be detectable in the vicinity of the Earth. For a typical interplanetary network detector sensitive to bursts of fluence 10^{-6} erg cm $^{-2}$ and above, PBH events could in principle be detected out to a distance of a few parsecs, depending on the emission model. PBHs evaporating today do not have enough luminosity to be detected at cosmological distances even by the most sensitive current instruments, so searching for them locally is a logical step.

When observed by a single detector, the properties of a PBH burst might not appear to be significantly different from those of other short bursts; instruments with localization or imaging capabilities would obtain their arrival directions as they would for an infinitely distant source. Indeed many attempts to find evidence for the existence of PBH bursts have to date been based mainly on the spatial distribution and time histories of a subset of short bursts (Cline and Hong 1996; Czerny et al. 1996; Cline et al. 1997, 1999, 2003, 2005; Czerny et al. 2011). Other search methods have employed atmospheric Cherenkov detectors (Porter and Weekes 1977, 1978, 1979; Linton et al. 2006; Tesic 2012; Glicenstein et al. 2013), air shower detectors (Fegan et al. 1978; Bhat et al. 1980; Alexandreas et al. 1993; Amenomori et al. 1995; Abdo et al. 2015), radio pulse detection (Phinney and Taylor 1979; Keane et al. 2012), spark chamber detection (Fichtel et al. 1994), and GRB femtolensing (Barnacka et al. 2012). Table 1 gives a comparison of these various methods.

To widely spaced interplanetary network (IPN) detectors, however, a local PBH burst could look significantly different when compared with bursts from distant sources, due to the curvature of the received wavefront. In this paper, we use this fact to explore the possibility that some short bursts may originate in the solar neighborhood, and estimate lower limits to the PBH burst evaporation rate assuming these bursts are real PBH bursts. This paper is organized as follows. In Section 2 we derive the fluence expected in the detector from a PBH burst using the standard emission model and, as a maximal alternative, the Hagedorn emission model. In Section 3 we explain how we localized the detected bursts in 3D relaxing the assumption that they are at infinite distances. The detailed discussion of the methodology is given in Appendix A. Our data selection criteria are described in Section 4. Our results and PBH burst rate limit calculation are given in Section 5. In Section 6, we discuss implications and limitations of our results.

2. PBH Burst Signatures

As a PBH Hawking-radiates, its mass is decreased by the total energy carried off by the emission, and the black hole temperature, which is inversely proportional to its mass, increases. In the standard emission model (SEM) (MacGibbon and Webber 1990), the black hole directly Hawking-radiates those particles which appear fundamental on the scale of the black hole. Once the black hole temperature reaches the QCD transition scale ($\sim 200 - 300$ MeV), quarks and gluons are directly Hawking-radiated. The PBH gamma-ray burst spectrum is the combination of the directly Hawking-radiated photons and those produced by the decay of other directly Hawking-radiated particles. An SEM PBH with a remaining emission lifetime of $\tau \lesssim 1$ sec has a mass of

$$M_{BH}(\tau) \approx 1.3 \times 10^9 \left(\frac{\tau}{1 \text{ s}} \right)^{1/3} \text{ g} \quad (1)$$

(Ukwatta et al. 2015) and a remaining rest mass energy of

$$E_{BH}(\tau) \approx 1.2 \times 10^{30} \left(\frac{\tau}{1 \text{ s}} \right)^{1/3} \text{ erg.} \quad (2)$$

The expected fluence arriving at the detector from a PBH at a distance d from Earth is then

$$F_D = \frac{E_{\gamma BH}}{4\pi d^2} \quad (3)$$

where $E_{\gamma BH} = \eta_{\gamma D} E_{BH}$ and $\eta_{\gamma D}$ is the fraction of the PBH energy that arrives in the energy band of the detector, and the maximum distance from which the SEM PBH is detectable is

$$d_{max} \simeq 0.01 \left(\frac{\eta_{\gamma D}}{10^{-2}} \right)^{1/2} \left(\frac{\tau}{1 \text{ s}} \right)^{1/6} \left(\frac{F_{D \text{ min}}}{10^{-6} \text{ erg cm}^{-2}} \right)^{-1/2} \text{ pc} \quad (4)$$

where $F_{D \text{ min}}$ is the sensitivity of the detector.

The SEM analysis is consistent with high energy accelerator experiments (MacGibbon et al. 2008). However, an alternative class of PBH evaporation models was proposed before the existence of quarks and gluons was confirmed in accelerator experiments and these models continue to be discussed in the PBH burst literature. In such models (which we label HM scenarios), a Hagedorn-type exponentially increasing number of degrees of freedom become available as radiation modes once the black hole temperature reaches a specific threshold such as the QCD transition scale. In the HM scenarios, we assume that the remaining PBH mass is emitted quasi-instantaneously as a burst of energy $E'_{BH} = M'_{BH} c^2$ once the black hole mass reaches some threshold M'_{BH} ; for the QCD transition scale, $M'_{BH} \sim 10^{14} \text{ g}$ and $E'_{BH} \sim 10^{35} \text{ erg}$. Proceeding as above, the maximum distance from which the HM PBH burst is detectable is

$$d'_{max} \simeq 9 \left(\frac{\eta'_{\gamma D}}{10^{-1}} \right)^{1/2} \left(\frac{M'_{BH}}{10^{14} \text{ g}} \right)^{1/2} \left(\frac{F_{D \text{ min}}}{10^{-6} \text{ erg cm}^{-2}} \right)^{-1/2} \text{ pc} \quad (5)$$

where $\eta'_{\gamma D}$ is the fraction of the HM PBH energy that arrives in the energy band of the detector.

3. Gamma-ray burst localization for a source at a finite distance

When a pair of IPN spacecraft detects a burst, if the distance to the source is taken to be a free parameter, the event is localized to one sheet of a hyperboloid of revolution about the axis defined by the line between the spacecraft. If the burst is assumed to be at a distance which is much greater than the interspacecraft distance, the hyperboloid intersects the celestial sphere to form the usual localization circle (or annulus, when uncertainties are taken into account). Another widely spaced spacecraft would produce a second hyperboloid which intersects the first one to define a locus of points which is a simple hyperbola. Note that both hyperboloids have a common focus. Again, if the burst is assumed to be at a large distance from the spacecraft, the hyperbola intersects the celestial sphere at two points to define two possible error boxes. A fourth, non-coplanar spacecraft even at a moderate distance from Earth, such as *Konus-WIND*, can often be used to eliminate one branch of the hyperbola and part of the second branch. A terrestrial analogue to this method is Time Difference of Arrival (TDOA), with the important exception that GRB sources can be at

distances which are effectively infinite. Further details are given in Appendix A. While a single instrument with imaging or localization capability would obtain the correct sky position for a PBH burst regardless of its distance, the same is not true of an IPN localization, for which the derived arrival direction depends on the source distance.

In this paper, we relax the assumption that bursts are at infinite distances. If a burst is detected by three widely spaced spacecraft, then according to the previous discussion, the possible location of the burst traces a simple hyperbola in space as illustrated in Figure 3. In an Earth-centered coordinate system, this hyperbola has a closest distance to the Earth, that is, a distance lower limit. As we explain in Section 5.2, this fact can be used to calculate a lower limit to the PBH burst density rate in the Solar neighborhood assuming that the bursts that we consider are actual PBH bursts. In principle, detections by three spacecraft can rule out a local origin for a burst, but it is impossible to prove a local origin with only three non-imaging spacecraft.

In the case where a burst is observed by four widely spaced non-imaging spacecraft, the burst can be localized to a single point in space (or a region in space if uncertainties are taken into consideration). This scenario is illustrated in Figure 4. Thus in order to prove the local origin of a burst using non-imaging spacecraft, one needs detections from at least four satellites that are at interplanetary distances from each other.

As mentioned in Appendix A, in the special case of two widely separated spacecraft, where one spacecraft has precise imaging capability, it is in principle possible to demonstrate a local origin. We have explored this case in detail and defer treatment of it to a future paper. None of the events in this paper are in that category.

4. Data Selection

The IPN database contains information on over 25,000 cosmic, solar, and magnetar events which occurred between 1990 and the present (<http://ssl.berkeley.edu/ipn3/index.html>). During this period, a total of 18 spacecraft participated in the network. Some were dedicated GRB detectors, while others were primarily gamma-ray detectors with GRB detection capability. Indeed, the composition of the IPN changed regularly during this time, as old missions were retired and new ones were launched. However, all the instruments were sensitive to bursts with fluences around 10^{-6} erg cm $^{-2}$ or peak fluxes ≥ 1 photon cm $^{-2}$ s $^{-1}$ and above, resulting in a roughly constant detection rate. All known bursts, regardless of their intensity or duration, or the instruments which detected them, are included in this list. We have searched it for gamma-ray bursts with the following properties.

- Confirmed cosmic bursts which occurred between 1990 October and 2014 December (24.25 y; 10795 GRBs survived this cut).
- Bursts observed by three or more spacecraft, of which two were at interplanetary distances;

839 GRBs survived this cut. This small number is due firstly to the relatively high sensitivity thresholds of the distant IPN detectors (roughly 10^{-6} erg cm $^{-2}$ or 1 photon cm $^{-2}$ s $^{-1}$), and their somewhat coarser time resolutions, and secondly to a 2.5 year period between 1993 August and 1996 February when there was only one interplanetary spacecraft in the network.

- Bursts with no X-ray or optical afterglow, either because there were no follow-up observations, or because searches were negative. In addition, as discussed before, the arrival direction derived from IPN localization depends on its assumed distance, and the bursts were initially triangulated assuming an infinite distance. Thus even if a simultaneous search had taken place, it might not have identified an event within the error box if the burst was local. Other selection effects come into play starting with the launch of the HETE spacecraft in 2000 October, and later with the launch of Swift in 2004 November, namely that X-ray and optical observations were often done rapidly, leading to more X-ray and optical detections and the elimination of the bursts from further consideration here. On the other hand, the launches of Suzaku in 2005 July and Fermi in 2008 June resulted in an increase in the short burst detection rate which more than compensated for the previous effect.
- Bursts with durations < 1 s and no extended emission (EE). No cut was made based on the light curve shape; we discuss this in section 6. The detection rate of short bursts was roughly, but not exactly, constant over the period of this study.

These cuts, which are commutative, were carried out in the order described above, so as to minimize the required analysis of the full sample of 10795 events. 36 bursts satisfied these criteria. None were detected by an imaging instrument with good spatial resolution. While we believe that the overall IPN detection rate of short bursts was roughly constant, the data selection resulted in a rate which varied significantly from year to year.

In order to obtain distance lower limits as described in Appendix A, these bursts were triangulated assuming that their distances from Earth were free parameters. In all cases, however, an infinite distance was also compatible with the data. The results appear in Table 2.

Of the 10795 GRBs which survived the first cut, we would expect roughly 20%, or 2150, to be short-duration events (< 1 s). Of those, perhaps 10%, or 215, would display extended emission (Pal’shin et al. 2013), bringing the sample to 1935 non-EE bursts. We would expect about 80% of them to have no optical counterpart, either because none was detected or none was searched for (this number applies only to short bursts). This reduces the sample to about 1550. Since only 36 events survived all the data cuts, we can estimate the average IPN efficiency for this selection procedure to be about 2.3%. Thus if we exclude the 2.5 year period when the IPN had a single interplanetary spacecraft, the observed event rate is 1.7/year, and the true rate is about 72/year.

5. Results

5.1. Distance Limits and Localizations of PBH Burst Candidates

According to the methodology described in Section 3 and Appendix A, we have calculated the minimum possible distances to the sample of 36 bursts selected in section 4. This burst sample is shown in Table 2 and the 12 columns give:

1. the date of the burst, in `yymmdd` format, with suffix A or B where appropriate,
2. the Universal Time of the burst at Earth, in seconds of day,
3. the spacecraft which were used for the triangulation; a complete list of the spacecraft which detected the burst may be found on the IPN website (<http://ssl.berkeley.edu/ipn3/index.html>),
4. the burst duration, in seconds,
5. the fluence of the burst in erg cm^{-2} ,
6. the energy range over which the duration and fluence were measured, in keV,
7. the lower limit to the burst distance, obtained by triangulation, in cm,
8. the distance to which this burst could have been detected if it were a PBH burst of energy 10^{34} erg, assuming that all the energy went into the measured fluence (this is essentially the maximum possible detectable distance),
9. the maximum detectable distance assuming the SEM model (Equation 4) in terms of the undetermined parameter $(\eta_{\gamma D})^{0.5}$,
10. the maximum detectable distance assuming the HM model (Equation 5) in terms of the undetermined parameter $(\eta'_{\gamma D})^{0.5}$,
11. whether or not counterpart searches took place and if so, their references,
12. references to the duration, peak flux, and/or fluence measurements, and/or to the localization.

The shortest burst in Table 2 has a duration of 60 ms. Due to the relatively coarse time resolutions of interplanetary detectors, bursts with shorter durations must have greater intensities to be detected, effectively setting a higher detection threshold for very short events. The weakest event has a fluence of $4.65 \times 10^{-7} \text{ erg cm}^{-2}$. The bursts in Table 2 could not have come from distances less than the distance lower limits in column 7; however, all of them have time delays which are also consistent with infinite distances. Figure 5 shows a histogram of these minimum distances. The detector-dependent distance upper limits in column 8 are calculated assuming the extreme case that these events are caused by $\sim 10^{34}$ erg HM-type bursts from primordial black

holes of mass $\sim 10^{14}$ g and that all of the emitted energy spectrum is contained within the detector measurement limits. Table 3 gives the coordinates of the centers and corners of the error boxes for the events in Table 2, assuming that the sources are at infinity. If in fact the sources are local, the arrival directions are distance-dependent, and different from the ones in Table 3. These coordinates represent the intersections of annuli, and in some cases the curvature of the annuli would make it inaccurate to construct an error box by connecting the coordinates with straight-line segments.

5.2. PBH Burst Density Rate Estimation

All previous direct PBH burst searches resulted in null detections (Abdo et al. 2015). In this case, one can derive an upper limit on the local PBH burst rate density, that is, an upper limit on the number of PBH bursts per unit volume per unit time in the local solar neighborhood.

However, in our case, we have PBH burst candidates with short duration, no known afterglow detection and minimum distances that are sub-light-years. Since we have PBH candidates, we should be able to derive an actual measurement of the PBH burst rate density under the assumption that the candidates are actual PBH bursts. Thus, the actual PBH burst rate density is

$$R = \frac{n}{VS\epsilon} \quad (6)$$

where n is the number of PBH bursts, V is the effective PBH detectable volume and S is the observed duration. The selection efficiency of the IPN is ϵ .

If all the candidates identified in Section 4 are real PBH bursts, then we have 36 PBH bursts, i.e., $n=36$. Hence, our PBH burst rate density estimate is,

$$R = \frac{36}{VS\epsilon}. \quad (7)$$

Next we need to estimate the values of S , V , and ϵ . Because we have studied IPN bursts collected over 21.75 years (the 2.5 year IPN non-sensitivity period is excluded), our observed duration is $S=21.75$ years. The effective PBH detectable volume, V , calculation for this 21.75 year period, however, is not obvious. Each PBH candidate has a distance consistent with some minimum distance up to infinity. We also know that PBH bursts are not bright enough to be detected from large distances. The maximum possible detectable distance of a PBH burst depends on the high-energy physics model used to calculate the final PBH burst spectrum (Ukwatta et al. 2015). Currently there are no accurate calculations for final PBH burst photon spectra in the keV-MeV energy range. Thus as a conservative maximum possible detectable PBH burst distance, we can take the maximum value of the minimum distances in our candidate PBH burst sample. This corresponds to a distance of 0.47 parsecs (1.5×10^{18} cm). Because all the PBH burst candidates in the sample are actual IPN detections, this distance value is model-independent. On the other hand, it is important to note that the IPN is not capable of detecting all the bursts within this distance

over the entire observation duration due to various factors such as the orientation of the satellites, and/or instrument duty cycles. Thus the effective volume calculated from the above maximum possible detectable PBH burst distance is an overestimate. Hence the PBH burst rate calculated in Equation 7 is in reality a lower limit on the PBH burst rate density,

$$R_{LL} = \frac{36}{VS\epsilon}. \quad (8)$$

In Section 4, we made a rough estimate of the selection efficiency of IPN, ϵ , for PBH bursts. However, we note that it is very challenging to calculate ϵ accurately due to a number of unknown factors such as the fraction of bursts without EE, the fraction of bursts without afterglows, the fraction of bursts to which the IPN is not sensitive (for example due to orientation or deadtime), etc.

Using the estimated effective PBH detectable volume V , observed duration S , and selection efficiency ϵ , we can now estimate the lower limit of the PBH burst rate in the best case scenario where all the PBH burst candidates are actual PBH bursts. In this case, our PBH burst lower limit is ~ 158.5 bursts $\text{pc}^{-3}\text{yr}^{-1}$. If we assumed 100% efficiency then the PBH burst lower limit is ~ 3.6 bursts $\text{pc}^{-3}\text{yr}^{-1}$. If only one of the candidates is an actual PBH burst then the value of the rate density lower limit depends on the minimum distance to that particular burst. If the burst with the largest minimum distance (GRB 140807) is the PBH burst, then the PBH burst rate density lower limit is ~ 0.1 bursts $\text{pc}^{-3}\text{yr}^{-1}$. If the burst with the smallest minimum distance (GRB 970902) is real then the PBH burst rate density lower limit is $\sim 1 \times 10^{14}$ bursts $\text{pc}^{-3}\text{yr}^{-1}$ (this value is excluded by other high-energy experiments, however). All these estimates assume that PBHs are distributed uniformly in the solar neighborhood. The IPN PBH burst rate density lower limit values are shown in Figure 6. PBH burst upper limits from various other searches are also shown in the figure.

In the worst case scenario where none of our candidates is a real PBH burst, we cannot estimate a lower limit to the PBH burst rate density and instead consider to estimate an upper limit to the PBH burst rate density. However, the assumption that none of the bursts in the sample is real but still we have candidates implies that our criteria to identify PBH bursts defined in section 4 is not sufficient. This means our method is not capable of setting an upper limit on the PBH burst rate density.

6. Discussion

The detection of gamma-ray transients points to very high energy explosive phenomena in the Universe. Their detection in the solar neighborhood would indicate a previously unrecognized and potentially exotic phenomenon in our cosmic backyard. The sample of bursts identified in this paper are candidates for such explosions. They have short durations, no known afterglow detections, and have distance limits consistent with the solar neighborhood. In principle our methodology is

capable of proving the local origin of bursts. However in order to do that we need either four widely separated non-imaging spacecraft or two spacecraft that include one with imaging capability (see Section 3 and Appendix A). This is not the case for any of the bursts we considered in our study. While some events were indeed detected by four or more spacecraft, the spacecraft were not widely separated, i.e. at interplanetary distances. With four widely separated non-imaging spacecraft detections or detections by one imaging spacecraft and one non-imaging spacecraft, it would be possible to prove that some of these bursts are in the solar neighborhood and this would definitely point to an exotic origin for these bursts. Lacking that however, we can look at other properties of these bursts and discuss how likely it is that they may have a PBH origin.

Firstly, it is of interest to investigate the sky distribution of our PBH burst candidates. For example, Cline et al. (1997) have argued that, due to the fact that very short duration GRBs (i.e., GRBs with duration ≤ 100 msec) have a non-isotropic sky distribution, they may be drawn from a different GRB population, possibly from PBH bursts. In order to investigate this we have calculated burst density maps using the Gaussian kernel density methodology described in Ukwatta & Woźniak (2016). Since the sky locations of the PBH candidates depends on their distance from earth, we started by assuming all the bursts are at their minimum distances and calculated their sky density map. This map is shown in Figure 7. The map is presented in Galactic coordinates with a 25 degree smoothing radius. It shows some relatively high density areas, but the probability of generating this density contrast by chance, in the case when the true sky distribution is uniform, is ~ 0.2 , estimated using a Monte Carlo simulation (Ukwatta & Woźniak 2016). Thus the density structure seen in Figure 7 is consistent with a uniform source distribution. If these PBH candidates are real, they cannot be further away than ~ 10 parsecs (which is the maximum possible distance they can be detected assuming the optimistic Hagedorn-type model). We then also calculated the sky locations of the PBH candidates assuming they are at 10 parsecs and derived the sky density map as shown in Figure 8. This map is also consistent with a uniform source distribution. This is the behaviour one would expect if these PBH burst are local with maximum detectable distance ~ 10 parsecs.

According to the standard model for Hawking radiation (MacGibbon and Webber 1990), PBH bursts are standard candles, that is, all PBH bursts are intrinsically identical at the source. However, the way the burst appears at large distances may vary depending on its host environment. The final burst properties of the PBH burst depend on its mass and the number of fundamental particle degrees of freedom available at various energies (Ukwatta et al. 2015). In principle, by measuring the photon flux arriving from a PBH burst candidate in a given energy range, we can calculate the distance to that burst. However, during the last second of the PBH lifetime, its temperature is well above ~ 1 TeV and the physics governing these high energies is not fully understood. Thus, the full spectrum of a PBH burst is difficult to calculate.

Ukwatta et al. (2015) have calculated PBH burst light curves in the 50 GeV – 100 TeV energy range using the Standard Model of particle physics. This calculation considered both the direct Hawking radiation of photons from the black hole and the photons created due to the fragmentation

and hadronization of the directly Hawking-radiated quarks and gluons. The expected PBH light curve is a power-law with an index of ~ 0.5 and at various sub-energy bands within the 50 GeV – 100 TeV energy range has an interesting inflection point due to the brief dominance of the directly Hawking-radiated photons around ~ 0.1 second before the PBH expiration. This is potentially a unique signature of a PBH burst in the GeV/TeV energy range.

The detectors in the IPN are sensitive to photons in the energy range 10 keV – 100 MeV. There are no published calculations of PBH burst light curves in the keV/MeV range using the Standard Model of particle physics to which we can fit our light curves and extract fit parameters. Nonetheless it is of interest to look at the light curves of our PBH burst candidates. Firstly, we note that, although a PBH will be emitting in the keV/MeV range before it becomes hot enough to emit in the GeV/TeV range, a keV/MeV burst signal can only be generated by the low energy component of a PBH that is also emitting in the GeV/TeV range: this is because a 10 TeV black hole has a remaining burst lifetime of ~ 1 s whereas a < 1 GeV black hole has a lifetime $\gg 10^4$ yr and observationally would be a stable source not a burst. This low energy photon component, in turn, is predominantly generated by other higher energy Hawking-radiated species via decays or the inner bremsstrahlung effect (Page et al. 2008) and is not the directly Hawking-radiated photon flux which decreases in the keV/MeV band as the burst progresses. Acknowledging the uncertainty in the PBH light curves in the keV/MeV range, it is also possible that the PBH burst signal may have a longer or shorter duration in the keV/MeV range than in the GeV/TeV range due to differences both in production at the source and in detector sensitivity, and that the duration difference varies with the distance to the PBH. Figure 9 shows the light curves of the 36 IPN bursts in our sample. Some are clearly single-peaked, others are clearly multi-peaked, and some were not recorded with sufficient statistics to determine the true number of peaks. It is interesting to note that bursts such as GRB 970921, GRB 080222, GRB000607, GRB 101009, GRB 121127, GRB 131126A, and GRB 141011A display a keV/MeV time profile that resembles the PBH light curve profile calculated by Ukwatta et al. (2015) for the GeV/TeV energy range.

In this paper, we introduced a novel method to constrain the distances to GRBs using detections from multiple spacecraft. Utilizing detections from three non-imaging spacecraft we could only constrain the minimum distances to our current sample of bursts. The maximum distance is constrained by the energy available during the final second of the PBH burst. However, the amount of energy released in the keV/MeV energy band is not known and may be highly model-dependent. On the other hand, with detections by four widely separated (\sim AU distances) non-imaging spacecraft or one non-imaging spacecraft and one imaging spacecraft, we can constrain burst distances independent of any high energy physics model, and potentially show that some bursts are local. Such a detection will not only prove the existence of PBH bursts, by fitting light curves and spectra derived using various beyond the standard model physics theories, we can also identify which theory describes nature.

7. Acknowledgments

Support for the IPN was provided by NASA grants NNX09AU03G, NNX10AU34G, NNX11AP96G, and NNX13AP09G (*Fermi*); NNG04GM50G, NNG06GE69G, NNX07AQ22G, NNX08AC90G, NNX08AX95G, and NNX09AR28G (INTEGRAL); NNX08AN23G, NNX09AO97G, and NNX12AD68G (*Swift*); NNX06AI36G, NNX08AB84G, NNX08AZ85G, NNX09AV61G, and NNX10AR12G (*Suzaku*); NNX07AR71G (MESSENGER); NAG5-3500, and JPL Contracts 1282043 and Y503559 (*Odyssey*); NNX12AE41G, NNX13AI54G, and NNX15AE60G (ADA); NNX07AH52G (Konus); NAG5-13080 (RHESI); NAG5-7766, NAG5-9126, and NAG5-10710, (*BeppoSAX*); and NNG06GI89G. TNU acknowledges support from the Laboratory Directed Research and Development program at the Los Alamos National Laboratory (LANL). The Konus-Wind experiment is partially supported by a Russian Space Agency contract and RFBR grants 15-02-00532 and 13-02-12017-ofi-m. We would also like to thank Jim Linnemann (MSU), Dan Stump (MSU), Brenda Dingus (LANL), and Pat Harding (LANL) for useful conversations on the analysis.

A. GRB triangulation when the source distance is allowed to vary

Assume two spacecraft, SC_1 and SC_2 , separated by a distance d , observe a GRB. For any assumed distance between the GRB and the spacecraft, the difference in arrival times δt_{12} must be constant. Let x_1, y_1, z_1 and x_2, y_2, z_2 be the coordinates of the two spacecraft. Then the locus of points x, y, z which describes the possible source locations is given by

$$\sqrt{(x - x_1)^2 + (y - y_1)^2 + (z - z_1)^2} - \sqrt{(x - x_2)^2 + (y - y_2)^2 + (z - z_2)^2} - c * \delta t_{12} = 0$$

where c is the speed of light.

Consider first the two-dimensional problem for simplicity. Let SC_1 and SC_2 define the z-axis of a coordinate system whose origin is halfway between the spacecraft. The positions of SC_1 and SC_2 are the foci of the hyperbola:

$$z^2/a^2 - x^2/b^2 = 1$$

This is shown in Figure 1. Here $2a$ is the difference between the distances of any point on the hyperbola from the foci, so $2a = c \delta t_{12}$, and $b = (d^2/4 - a^2)^{1/2}$. For every point on this hyperbola, the difference in the arrival times is δt_{12} . If we assume an infinite distance for the source, the asymptotes of the hyperbola define the two possible arrival directions of the GRB.

Now consider the three-dimensional case. If we rotate the hyperbola of Figure 1 about the z axis, we obtain one sheet of a hyperboloid of rotation of two sheets. Its formula is

$$-x^2/b^2 + z^2/a^2 - y^2/b^2 = 1.$$

Here, the x axis is perpendicular to the y and z axes, and cuts in the plane z=constant give circles. This is illustrated in Figure 2.

In practice, we will have two or more hyperboloids generated by three or more spacecraft, and we will want to work in Earth-centered Cartesian coordinates with one axis oriented towards right ascension zero, declination zero, and another axis oriented towards declination 90°. Consider the three-spacecraft case. A spacecraft pair will define two foci of a hyperboloid; the line joining the two spacecraft, which defines the axis of rotation of the hyperboloid, will be oriented with respect to Earth-centered coordinates such that it represents a rotation and a translation. We want to express the formula for the hyperboloid in the Earth-centered system.

The coordinate rotation can be described by three sets of direction cosines:

$$\begin{aligned} z' &= x * \cos(\alpha z_{12}) + y * \cos(\beta z_{12}) + z * \cos(\gamma z_{12}) \\ y' &= x * \cos(\alpha y_{12}) + y * \cos(\beta y_{12}) + z * \cos(\gamma y_{12}) \\ x' &= x * \cos(\alpha x_{12}) + y * \cos(\beta x_{12}) + z * \cos(\gamma x_{12}) \end{aligned}$$

Here the primed coordinate system is the one defined by the foci of the hyperboloid; its origin is the same as that of the unprimed, Earth-centered system, and it is rotated, but not translated, with respect to it. Now perform a translation of the primed system so that its origin is at the midpoint of the two foci. If the coordinates of the two spacecraft, expressed in the unprimed system, are x_1, y_1, z_1 and x_2, y_2, z_2 , the origin of the translated system will be at $(x_1 + x_2)/2, (y_1 + y_2)/2, (z_1 + z_2)/2$. The formula for the hyperboloid, expressed in the Earth-centered system, becomes

$$\begin{aligned} &(x_1 * \cos(\alpha z_{12}) + x_2 * \cos(\alpha z_{12}) + y_1 * \cos(\beta z_{12}) + y_2 * \cos(\beta z_{12}) + z_1 * \cos(\gamma z_{12}) + \\ &\quad z_2 * \cos(\gamma z_{12}) - 2 * x * \cos(\alpha z_{12}) - 2 * y * \cos(\beta z_{12}) - 2 * z * \cos(\gamma z_{12}))^2 / (4 * a_{12}^2) \\ &- (x_1 * \cos(\alpha x_{12}) + x_2 * \cos(\alpha x_{12}) + y_1 * \cos(\beta x_{12}) + y_2 * \cos(\beta x_{12}) + z_1 * \cos(\gamma x_{12}) + \\ &\quad z_2 * \cos(\gamma x_{12}) - 2 * x * \cos(\alpha x_{12}) - 2 * y * \cos(\beta x_{12}) - 2 * z * \cos(\gamma x_{12}))^2 / (4 * b_{12}^2) \\ &- (x_1 * \cos(\alpha y_{12}) + x_2 * \cos(\alpha y_{12}) + y_1 * \cos(\beta y_{12}) + y_2 * \cos(\beta y_{12}) + z_1 * \cos(\gamma y_{12}) + \\ &\quad z_2 * \cos(\gamma y_{12}) - 2 * x * \cos(\alpha y_{12}) - 2 * y * \cos(\beta y_{12}) - 2 * z * \cos(\gamma y_{12}))^2 / (4 * b_{12}^2) - 1 = 0 \end{aligned}$$

where a_{12} and b_{12} refer to the hyperboloid for spacecraft 1 and 2. A similar equation describes the hyperboloid for spacecraft 1 and 3. Although a third equation can be derived for spacecraft 2 and 3, it is not independent of the other two, because it is constrained by the condition $\delta t_{12} + \delta t_{13} + \delta t_{32} = 0$.

The locus of points describing the intersection of two hyperboloids is a simple hyperbola, contained in a plane. This is shown in Figure 3. This hyperbola contains all the points satisfying the time delays for the two spacecraft pairs, δt_{12} and δt_{13} , when the GRB distance is allowed to vary. The two branches of the hyperbola intersect the celestial sphere at two points; if the distance is taken to be infinite, the two points are the possible source locations. It follows that a GRB observed by three, and only three, widely separated non-imaging spacecraft, cannot be unambiguously proven to originate at a local distance; on the other hand, in the case where the hyperbola degenerates to a single point, that point must be at an infinite distance, and a local origin can be ruled out. None of the bursts in this sample were in this category.

In the simplest case, we have one spacecraft near Earth, and two spacecraft in interplanetary space. So

$$\sqrt{(x - x_1)^2 + (y - y_1)^2 + (z - z_1)^2} - \sqrt{(x - x_2)^2 + (y - y_2)^2 + (z - z_2)^2} - c * \delta t_{12} = 0 \quad (\text{A1})$$

$$\sqrt{(x - x_1)^2 + (y - y_1)^2 + (z - z_1)^2} - \sqrt{(x - x_3)^2 + (y - y_3)^2 + (z - z_3)^2} - c * \delta t_{13} = 0 \quad (\text{A2})$$

The lower limit to the source distance is the point on the hyperbola (x, y, z) which is closest to Earth. This can be found by solving for the minimum of the expression $\sqrt{x^2 + y^2 + z^2}$ (the Earth distance) subject to the constraints imposed by equations A1 and A2. In practice there are uncertainties associated with δt_{12} and δt_{13} , and we have used the most probable values to derive the lower limits. Since x , y , and z vary along the hyperbola, the apparent arrival direction for an observer at Earth depends on the assumed distance; if the source distance is assumed to be infinite, the derived right ascension and declination will not be correct if the source is actually local. For example, if GRB 140807 were at its minimum allowable distance (1.46×10^{18} cm, or 9.8×10^4 AU), the angle between its true coordinates and the coordinates for an infinitely distant source would be 0.04° . But for GRB 101129, whose minimum allowable distance is only 3.89×10^{13} cm, or 2.6 AU, the angle would be 54.2° .

In a number of cases, a fourth non-coplanar experiment, in this case *Konus-Wind*, at up to 7 light-seconds from Earth, can be used to constrain the lower limits further. Adding the constraint

$$\sqrt{(x - x_1)^2 + (y - y_1)^2 + (z - z_1)^2} - \sqrt{(x - x_4)^2 + (y - y_4)^2 + (z - z_4)^2} - c * \delta t_{14} = 0$$

eliminates one branch of the hyperbola and part of the second branch, leading to a larger distance lower limit. Thus, in the case of four widely separated spacecraft, it is in principle possible to rule out an infinite distance and prove that the origin is local as illustrated in Figure 4. However, this was not the case for any of the bursts in this study; they are all consistent with both local and infinite distances.

Note that this method does not depend on the properties of the GRB itself, such as duration or intensity; the lower limit is determined by the IPN configuration (through the spacecraft coordinates) and the direction of the burst (through the time delays). Thus, for example, it can be applied equally to long- and short-duration bursts, and a sample of long-duration events would yield a distribution of lower limits which was comparable to a sample of short-duration events.

One special case should be noted here. With just two widely separated spacecraft, if one has precise imaging capability, the problem reduces to finding the intersection of a hyperboloid and the vector defined by the precise localization from the imager. In principle, a local origin can be demonstrated, or a distance lower limit can be obtained. We have studied approximately two hundred GRBs which are in this category, and analysis of the results is ongoing.

REFERENCES

- Abdo, A. A., Abeysekara, A. U., Alfaro, R., et al. 2015, *Astroparticle Physics*, 64, 4
- D. E. Alexandreas, G. E. Allen, D. Berley, et al. 1993, *Physical Review Letters* 71, 2524
- M. Amenomori, Z. Cao, B. Z. Dai, et al. 1995, *Proc. International Cosmic Ray Conference* 2, 112
- Barnacka, A., Glicenstein, J.-F., and Moderski, R. 2012 *Phys. Rev. D* 86, 043001
- Bhat, P., Gopalakrishnan, N., Gupta, S., Ramana Murthy, P., Sreekantan, B., and Tonwar, S. 1980
Nature 284, 433
- Cline, D. & Hong, W. 1996, *Astroparticle Physics* 5, 175
- Czerny, B., et al. 2011, *New Astronomy* 16, 33
- Cline, D., et al. 1997, *ApJ* 486, 169
- Cline, D., et al. 1999, *ApJ* 527, 827
- Cline, D., et al. 2003, *Astroparticle Physics* 18, 531
- Cline, D., et al. 2005, *ApJ* 633, L73
- Czerny, B., et al. 2011, *New Astronomy* 16, 33
- Cline, D. & Hong, W. 1992, *ApJ* 401, L57
- Eichler, D., Livio, M., Piran, T., and Schramm, D. 1989, *Nature* 340, 126
- Fegan, D., McBreen, B., O’Brien, D., and O’Sullivan, C. 1978, *Nature* 271, 731
- Fichtel, C., Bertsch, D., Dingus, B., et al. 1994, *ApJ* 434, 557
- Frontera, F., Guidorzi, C., Montanari, E., et al. 2009, *ApJS* 180, 192
- J. Glicenstein, A. Barnacka, M. Vivier, et al. 2013, arXiv:1307.4898
- Goldstein, A., Burgess, J. M., Preece, R., et al. 2012 *ApJS* 199, 19
- Goldstein, A., Preece, R., Mallozzi, R., et al. 2013 *ApJS* 208, 21
- Golenetskii, S., Aptekar, R., Mazets, E., et al. 2011a, *GCN Circ.* 12110
- Golenetskii, S., Aptekar, R., Frederiks, D., et al. 2011b, *GCN Circ.* 12111
- Golenetskii, S., Aptekar, R., Frederiks, D., et al. 2011c, *GCN Circ.* 12249
- Golenetskii, S., Aptekar, R., Frederiks, D., et al. 2011d, *GCN Circ.* 12271

- Golenetskii, S., Aptekar, R., Mazets, E., et al., 2012a GCN Circ. 13313
- Golenetskii, S., Aptekar, R., Frederiks, D., et al. 2012b, GCN Circ. 13315
- Golenetskii, S., Aptekar, R., Mazets, E., et al. 2012c, GCN Circ. 13620
- Golenetskii, S., Aptekar, R., Frederiks, D., et al. 2012d, GCN Circ. 13621
- Golenetskii, S., Aptekar, R., Mazets, E., et al. 2012e, GCN Circ. 13627
- Golenetskii, S., Aptekar, R., Mazets, E., et al. 2012f, GCN Circ. 14021
- Golenetskii, S., Aptekar, R., Frederiks, D. et al. 2012g, GCN Circ. 14022
- Golenetskii, S., Aptekar, R., Mazets, E., et al. 2013a, GCN Circ. 14561
- Golenetskii, S., Aptekar, R., Frederiks, D., et al. 2013b, GCN Circ. 14565
- Golenetskii, S., Aptekar, R., Pal'shin, V., et al. 2013c, GCN Circ. 15550
- Golenetskii, S., Aptekar, R., Frederiks, D., et al. 2013d, GCN Circ. 15551
- Golenetskii, S., Aptekar, R., Mazets, E., et al. 2014a, GCN Circ. 16801
- Golenetskii, S., Aptekar, R., Frederiks, D., et al. 2014b, GCN Circ. 16807
- Golenetskii, S., Aptekar, R., Pal'shin, V., et al. 2014c, GCN Circ. 16906
- Golenetskii, S., Aptekar, R., Frederiks, D., et al. 2014d, GCN Circ. 16907
- Guiriec, S., Briggs, M., Connaughton, V., et al. 2010, ApJ 725, 225
- Hawking, S. 1974, Nature 248, 30
- Hurley, K., Berger, E., Castro-Tirado, A., et al. 2002, ApJ 567,447
- Hurley, K., Rowlinson, A., Bellm, E., et al. 2010, MNRAS 403, 342
- Hurley, K., Goldsten, J., Mitrofanov, I., et al. 2011a, GCN Circ. 12247
- Hurley, K., Goldsten, J., Mitrofanov, I., et al. 2011b, GCN Circ. 12269
- Ishida, Y., Tashiro, M., Terada, Y., et al. 2012, GCN Circ. 14044
- Jelley, J., Baird, G., and O'Mongain, E. 1977, Nature 267, 499
- Keane, E., Stappers, B., Kramer, M., and Lyne, A. 2012, MNRAS 425, L71
- E. T. Linton, R. W. Atkins, H. M. Badran, et al. 2006, JCAP 1, 13
- MacGibbon, J. H. and Webber, B. R. 1990 Phys. Rev. D 41, 3052

- MacGibbon, J. H., Carr, B. J., & Page, D. N. 2008, *Phys. Rev. D* 78, 064043
- Masetti, N., Palazzi, E., Pian, E., et al. 2000, *GCN Circ.* 720
- Mazets, E., Aptekar, R., Cline, T., et al. 2008, *ApJ* 680, 545
- Paciesas, W., Meegan, C., Pendleton, G., et al. 1999 *ApJS* 122, 465
- Paciesas, W., Meegan, C., von Kienlin, A., et al. 2012 *ApJS* 199, 18
- Pagani, C., and Evans, P. A. 2014, *GCN Circ.* 17134
- Page, D. & Hawking, S. 1976, *ApJ* 206, 1
- Page, D. 1976, *Phys. Rev. D* 13, 198
- Page, D. N., Carr, B. J., & MacGibbon, J. H. 2008, *Phys. Rev. D*, 78, 064044
- Pal'shin, V., Hurley, K., Svinkin, D., et al. 2013, *ApJS* 207, 38
- Park, H., Williams, G., Perez, D., et al. 2000, *GCN Circ.* 873
- Pelassa, V., and Meegan, C. 2013, *GCN Circ.* 15573
- Phinney, S., and Taylor, J. 1979 *Nature* 277, 117
- Porter, N., and Weekes, T. 1977 *ApJ* 212, 224
- Porter, N., and Weekes, T. 1978 *MNRAS* 183, 205
- Porter, N., and Weekes, T. 1979 *Nature* 277, 199
- Price, P., Axelrod, T., and Schmidt, B. 2000, *GCN Circ.* 898
- Rees, M. 1977, *Nature* 266, 333
- Sakamoto, A., Tashiro, M., Terada, Y., et al. 2012, *GCN Circ.* 13350
- Singer, L., Kasliwal, M., and Cenko, S. 2013, *GCN Circ.* 15572
- Singer, L., private communication 2014
- Svinkin, D., Hurley, K., Aptekar, R., et al. 2015a, *MNRAS* 447, 1028
- Svinkin, D., et al. 2015b, in preparation
- Terekhov, O., Denisenko, D., Lobachev, V., et al. 1994, *Astron. Lett.* 20(3), 265
- G. Tesic and VERITAS Collaboration 2012, *Journal of Physics Conference Series* 375 052024
- Ukwatta, T. N., & Woźniak, P. R. 2016, *MNRAS*, 455, 703

Ukwatta, T. N., Stump, D., MacGibbon, J. H., et al. 2015, arXiv:1510.04372

von Kienlin, A., Meegan, C., Paciesas, W., et al. 2014 ApJS 211, 13

von Kienlin, A. 2013, GCN Circ. 14560

von Kienlin, A. 2014, GCN Circ. 16905

Vreeswijk, P., and Rol, E. 2000, GCN Circ. 908

Xiong, S. Meegan C. 2012, GCN Circ. 13644

Yasuda, T., Terada, Y., Tashiro, M., et al. 2011, GCN Circ. 12114

Yasuda, T., Tashiro, Y., Terada, Y., et al. 2013, GCN Circ. 14600

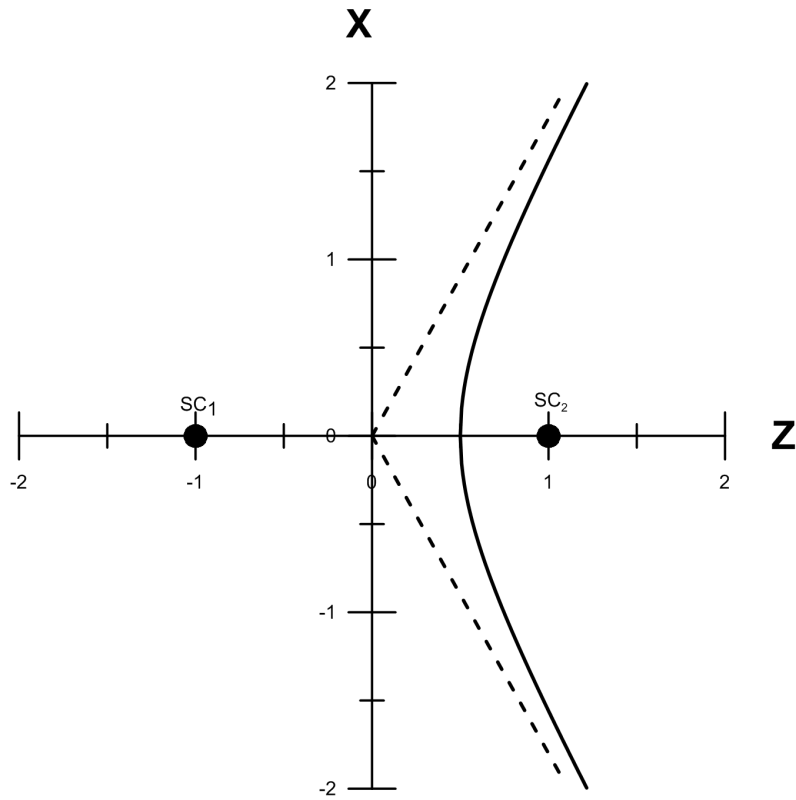


Fig. 1.— A two-dimensional example of GRB triangulation when the source distance is allowed to vary. The two spacecraft, 1 and 2, are aligned along the z -axis, and are the foci of a hyperbola. The hyperbola defines the loci of possible source distances. If the distance is assumed to be infinite, the two possible GRB arrival directions are along the asymptotes (dashed lines).

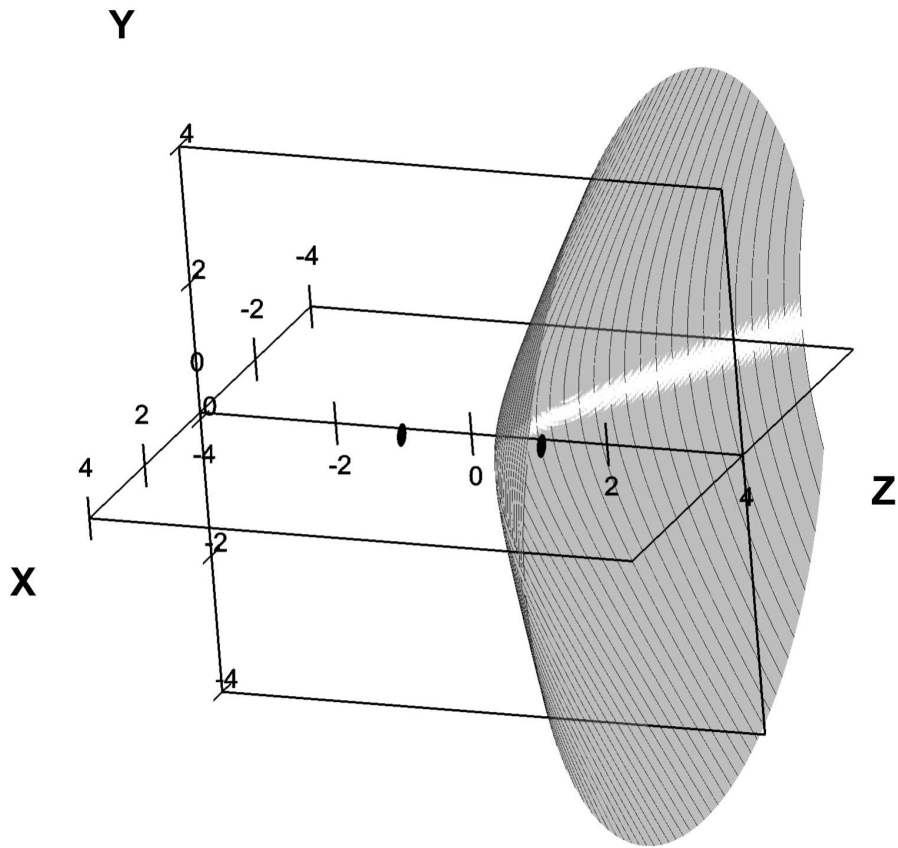


Fig. 2.— The hyperbola of Figure 1 rotated to obtain one sheet of a hyperboloid of rotation of two sheets. The two spacecraft are aligned along the z-axis, and are the foci of the hyperboloids. Each hyperboloid defines the loci of possible source distances in the three-dimensional problem. If the distance is assumed to be infinite, the circle defined by the intersection of the hyperboloid with the celestial sphere gives the possible GRB arrival directions.

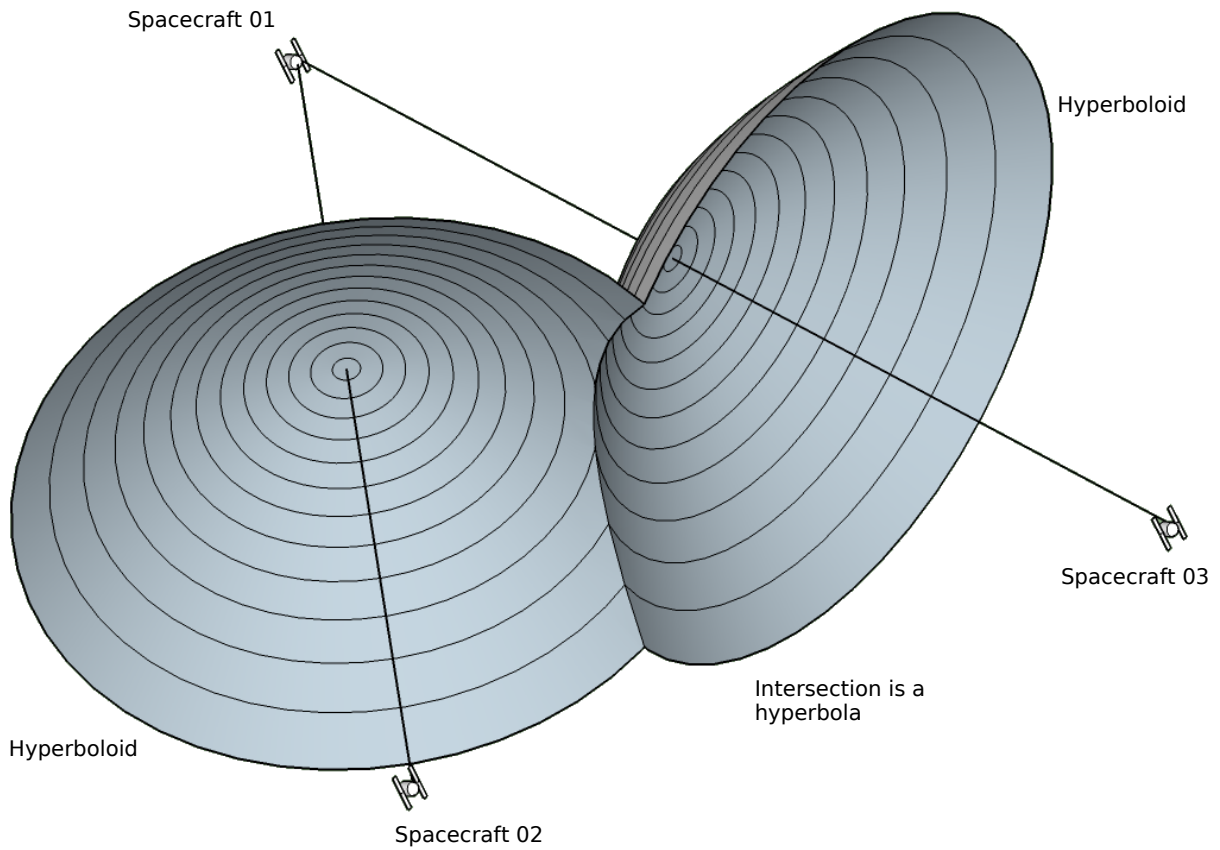


Fig. 3.— The intersection of two hyperboloids. With detections with three spacecraft, each spacecraft pair constrain the location of the source to a surface of a hyperboloid. The intersection of the two hyperboloids is a simple hyperbola contained in a plane. The point on this hyperbola which is closest to Earth gives the lower limit to the source distance.

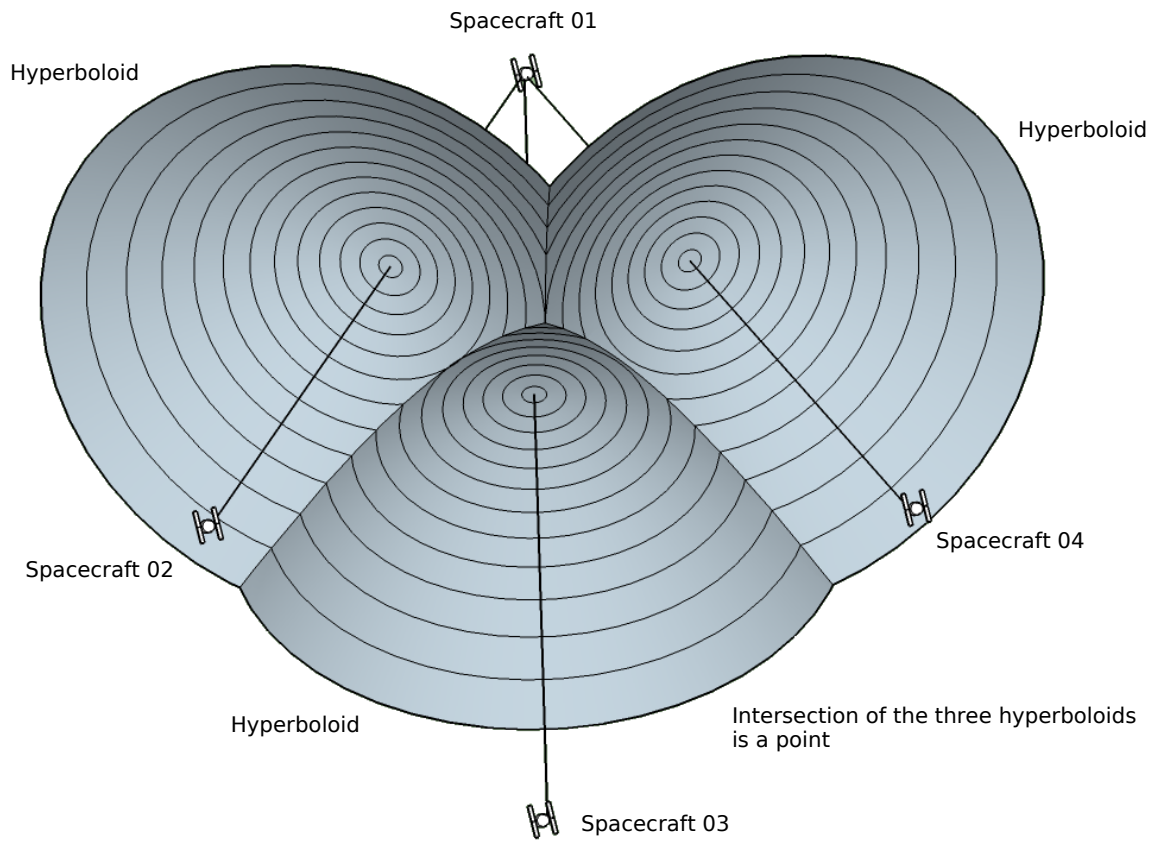


Fig. 4.— The intersection of three hyperboloids. With detections with four widely separated spacecraft, each spacecraft pair constrain the location of the source to a surface of a hyperboloid. The intersection of the three hyperboloids is a point in space as illustrated in the figure. In this case one can determine the source distance purely by timing measurements.

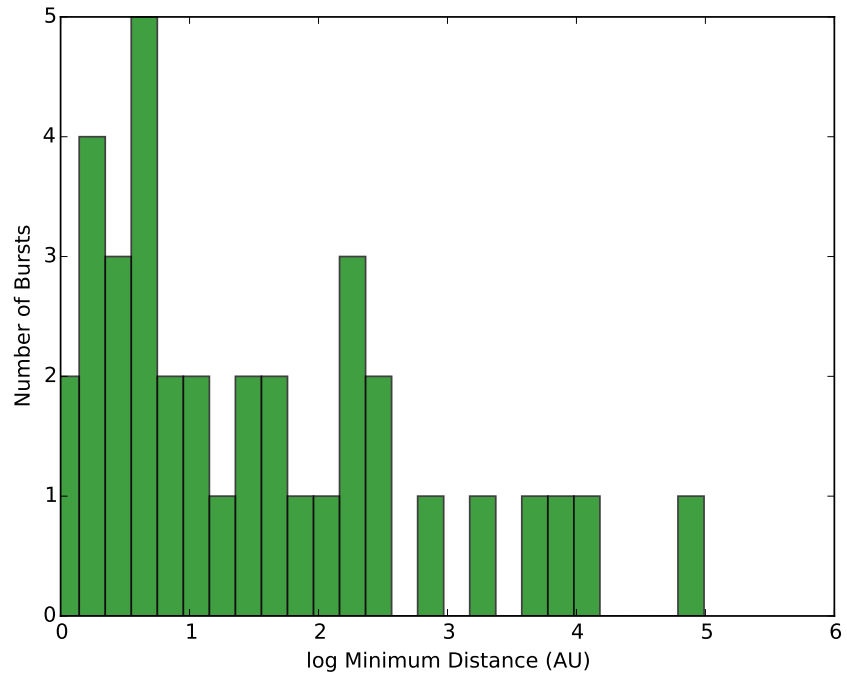


Fig. 5.— Histogram of the minimum distances to the PBH burst candidates in the IPN sample.

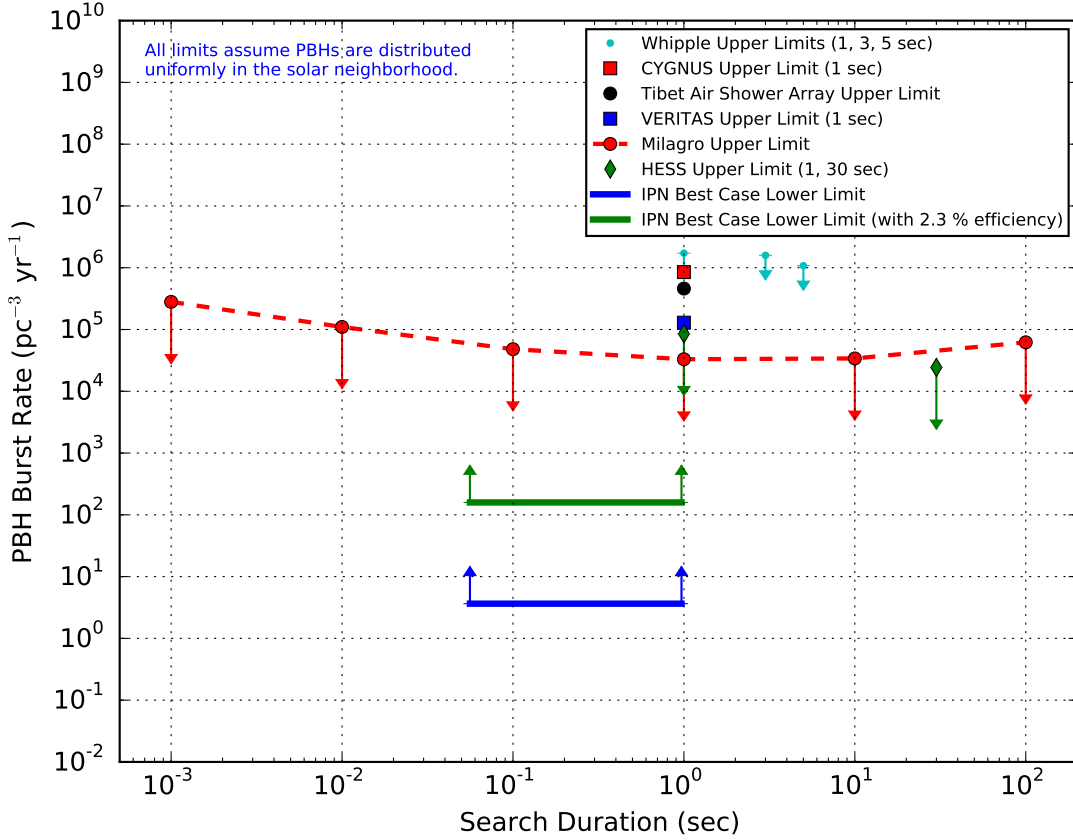


Fig. 6.— IPN PBH burst rate lower limit estimates assuming all the candidates are real PBH bursts. The horizontal green line gives the IPN PBH burst rate lower limit considering the selection efficiency of 2.3%. The blue horizontal line shows the lower limit if we assume 100% selection efficiency. Published PBH burst rate upper limits for various other burst search experiments are shown for comparison (Alexandreas et al. 1993; Amenomori et al. 1995; Linton et al. 2006; Tesic 2012; Glicenstein et al. 2013; Abdo et al. 2015).

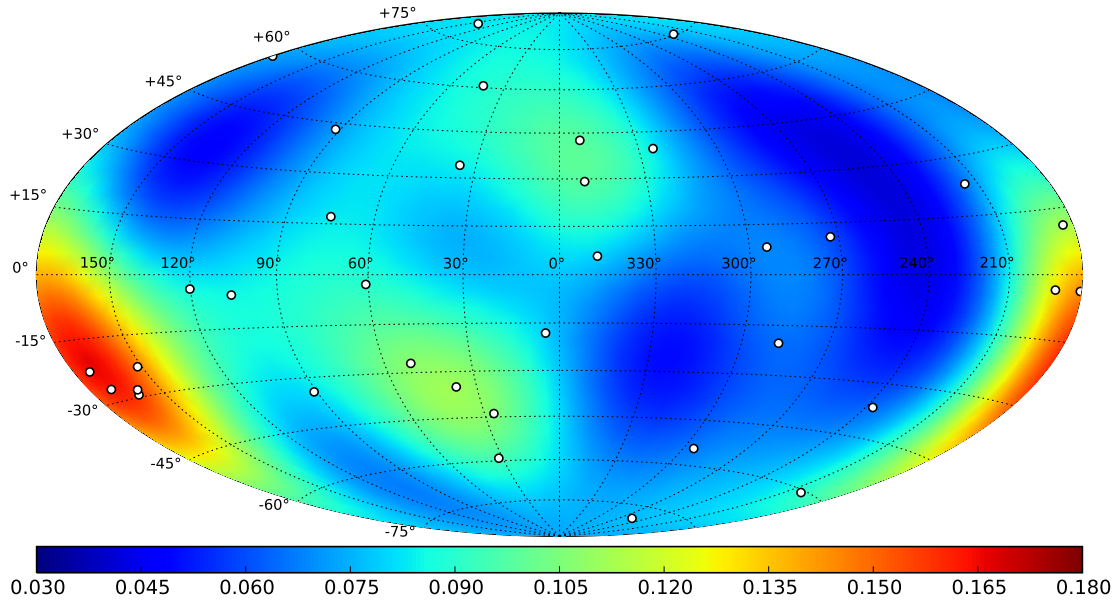


Fig. 7.— GRB density map in Galactic coordinates for the PBH burst candidates assuming minimum distances given in Table 2. This map is normalized to represent a probability density function (PDF) that integrates to 1 over the entire sphere. The smoothing parameter is taken to be 25 degrees. The circles indicate the locations of the individual bursts. The maximum and the minimum density values in this map are 0.166 and 0.041, respectively. The probability of generating this density contrast by chance in the case when the true sky distribution is uniform, is ~ 0.2 estimated using a Monte Carlo simulation (Ukwatta & Woźniak 2016). Thus the density structures seen in the map are consistent with a uniform distribution.

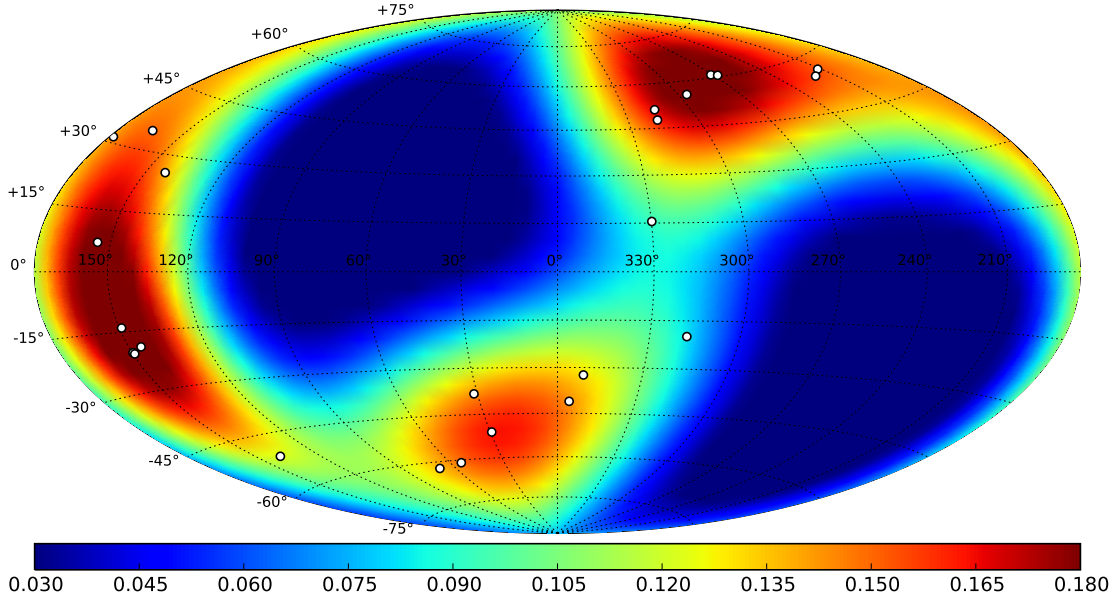


Fig. 8.— GRB density map in Galactic coordinates for the PBH burst candidates assuming constant distances of 10 parsecs to sources. The map has only 24 candidates with four spacecraft detections. Remaining 8 bursts have only three spacecraft detections, so they don't have a single localization. This map is normalized to represent a probability density function (PDF) that integrates to 1 over the entire sphere. The smoothing parameter is taken to be 25 degrees. The circles indicate the locations of the individual bursts. The maximum and the minimum density values in this map are 0.202 and 0.002, respectively. The probability of generating this density contrast by chance in the case when the true sky distribution is uniform, is ~ 0.1 estimated using a Monte Carlo simulation (Ukwatta & Woźniak 2016). Thus the density structures seen in the map are consistent with a uniform distribution.

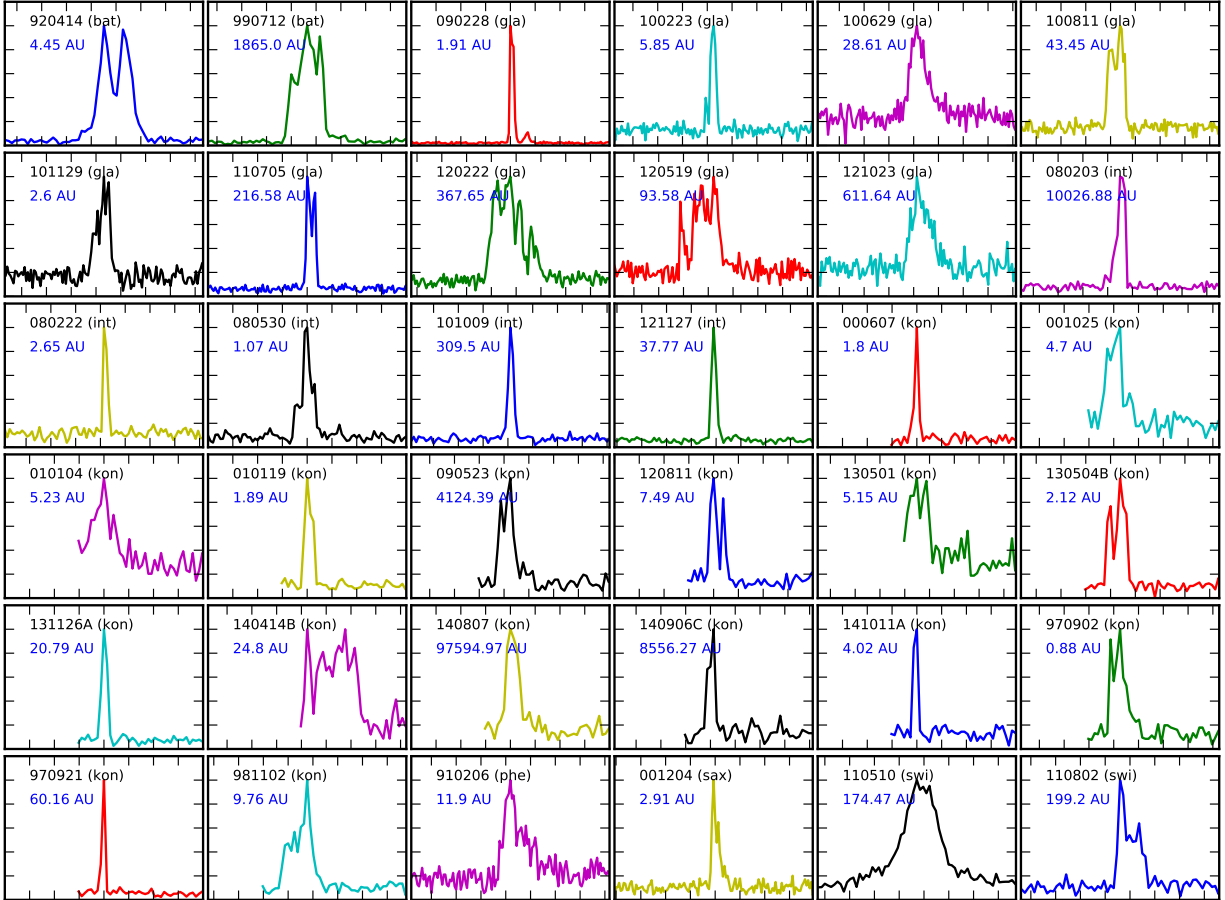


Fig. 9.— Normalized light curves of all the PBH burst candidates in the IPN sample. Black labels show the burst name with parenthesis showing the instrument. The blue labels give the minimum distance to the bursts based on our analysis. Each light curve shows a time range of 4 seconds centered on the brightest peak.

Table 1. Comparison of methods used to detect PBH evaporations.

Method	Burst duration, s	Energy or frequency	Rate upper limits, $\text{pc}^{-3} \text{y}^{-1}$	References
Atmospheric Cherenkov	$10^{-7} - 0.1$	200 MeV-10 TeV	$0.04 - 8.7 \times 10^5$	1
Air Shower	$10^{-6} - 0.1$	$5 \times 10^{12} - \gtrsim 5 \times 10^{13}$ eV	$2.7 \times 10^3 - 6 \times 10^3$	2
Radio Pulse	$< 3 \times 10^{-3}$	430-1374 MHz	2×10^{-9}	3
Spark Chamber	10^{-6}	20 MeV-1 GeV	5×10^{-2}	4
Spatial Distribution	< 0.1	15 keV-10 MeV	...	5

References. — (1) Porter and Weekes (1977, 1978, 1979); Abdo et al. (2015); (2) Bhat et al. (1980); Fegan et al. (1978); (3) Phinney and Taylor (1979); Keane et al. (2012); (4) Fichtel et al. (1994); (5) Cline and Hong (1996); Czerny et al. (1996); Cline et al. (1997, 1999, 2003, 2005); Czerny et al. (2011)

Table 2. Distance lower limits for IPN gamma-ray bursts.

GRB	SOD	Spacecraft ^a	Dur., s	Fluence erg cm ⁻²	Energy range, keV	Minimum Distance, cm.	Maximum detectable dist., cm.	Maximum detectable dist., (η_{rD}) ^{0.5} cm. (SEM Model)	Maximum detectable dist., (η'_{rD}) ^{0.5} cm. (HM Model)	Counterpart search?	Refs.
910206	31529	Uly,PVO,Phc	0.7	1.1×10^{-5}	100-100000	1.8×10^{14}	8.5×10^{18}	8.8×10^{16}	2.6×10^{19}	No	1,6
920414	84162	Uly,BAT,PVO	0.96	5.8×10^{-6}	20-2000	6.7×10^{13}	1.2×10^{19}	1.3×10^{17}	3.7×10^{19}	No	2,3,6
970902	27561	Uly,Kon,NEAR	0.44	4.2×10^{-6}	10-10000	1.3×10^{13}	1.4×10^{19}	1.3×10^{17}	4.3×10^{19}	No	4,5
970921	83828	Uly,Kon,NEAR	0.06	2.9×10^{-6}	10-10000	9.0×10^{14}	1.6×10^{19}	1.1×10^{17}	5.1×10^{19}	No	4,5
981102	28554	Uly,Kon,NEAR	0.57	1.1×10^{-5}	10-10000	1.5×10^{14}	8.5×10^{18}	8.5×10^{16}	2.7×10^{19}	No	5,13
990712	27919	Uly,BAT,Kon,NEAR	0.62	2.1×10^{-5}	10-10000	2.8×10^{16}	1.3×10^{19}	6.2×10^{16}	1.9×10^{19}	No	5,8
000607	08689	Uly,Kon,NEAR	0.09	4.6×10^{-6}	10-10000	2.7×10^{13}	1.4×10^{19}	9.6×10^{16}	4.1×10^{19}	14,15	5,13
001025	71369	Uly,Kon,NEAR	0.48	4.9×10^{-6}	10-10000	7.0×10^{13}	1.4×10^{19}	1.2×10^{17}	4.0×10^{19}	15,16	5,13
001204	28869	Uly,Kon,SAX,NEAR	0.27	1.1×10^{-6}	10-10000	4.4×10^{13}	3.0×10^{19}	2.4×10^{17}	8.4×10^{19}	15,17,18	5,7,13
010104	62490	Uly,Kon,SAX,NEAR	0.76	6.6×10^{-7}	10-10000	7.8×10^{13}	3.6×10^{19}	3.6×10^{17}	1.1×10^{20}	No	5,7,13
010119	37177	Uly,Kon,NEAR	0.18	2.3×10^{-6}	10-10000	2.8×10^{13}	1.9×10^{19}	1.5×10^{17}	5.8×10^{19}	No	5,7,13
080203	08456	Ody,Kon,INT,MES	0.4	9.3×10^{-6}	10-10000	1.5×10^{17}	9.8×10^{18}	8.7×10^{16}	2.9×10^{19}	No	5,13
080222	37262	Ody,Kon,MES	0.11	1.9×10^{-6}	10-10000	4.0×10^{13}	2.1×10^{19}	1.6×10^{17}	6.4×10^{19}	No	5,13
080530	58296	Ody,INT,MES,Suz	0.41	1.0×10^{-6}	100-1000	1.6×10^{13}	2.8×10^{19}	2.6×10^{17}	8.7×10^{19}	No	6
090228	17600	Ody,Kon,RHE,MES	0.08	6.3×10^{-6}	10-10000	2.9×10^{13}	1.1×10^{19}	8.1×10^{16}	3.5×10^{19}	No	5,6,9,10,19
090523	34075	Ody,Kon,MES,Suz	0.5	1.6×10^{-6}	10-10000	6.2×10^{16}	2.3×10^{19}	2.2×10^{17}	6.9×10^{19}	No	5,6,13
100223	09491	Ody,Kon,MES,Suz	0.19	1.7×10^{-6}	10-10000	8.8×10^{13}	2.3×10^{19}	1.8×10^{17}	6.7×10^{19}	No	5,6,9,10
100629	69243	Ody,Kon,INT,MES	0.46	1.1×10^{-6}	10-10000	4.3×10^{14}	2.6×10^{19}	2.6×10^{17}	8.5×10^{19}	No	5,6,9,10
100811	09349	Ody,Kon,INT,MES	0.33	4.4×10^{-6}	10-10000	6.5×10^{14}	1.6×10^{19}	1.2×10^{17}	4.2×10^{19}	No	5,6,9,11
101009	24858	Ody,Kon,INT,MES	0.18	1.6×10^{-6}	10-10000	4.6×10^{15}	1.6×10^{19}	1.8×10^{17}	6.9×10^{19}	No	5,6,13
101129	56371	Ody,Kon,INT,MES	0.32	3.7×10^{-6}	10-10000	3.9×10^{13}	3.0×10^{19}	1.3×10^{17}	4.6×10^{19}	No	5,9,11
110510	80844	Ody,Kon,Swi,MES	0.84	9.7×10^{-7}	10-10000	2.6×10^{15}	3.1×10^{19}	3.0×10^{17}	8.9×10^{19}	No	6,13
110705	13031	Ody,Kon,INT,MES	0.22	5.7×10^{-6}	10-10000	3.2×10^{15}	1.7×10^{19}	1.0×10^{17}	3.7×10^{19}	No	9,11,20,21,22
110802	55157	Ody,Kon,INT,MES	0.54	1.3×10^{-5}	10-10000	3.0×10^{15}	7.8×10^{18}	7.6×10^{16}	2.4×10^{19}	No	13,23,24
120222	01776	Ody,Kon,MES,Fer	0.87	1.8×10^{-6}	10-10000	5.5×10^{15}	2.1×10^{19}	2.3×10^{17}	6.6×10^{19}	No	9,11
120519	62294	Ody,Kon,MES,Fer	0.91	3.6×10^{-6}	10-10000	1.4×10^{15}	1.8×10^{19}	1.6×10^{17}	4.6×10^{19}	No	9,11,25,26,27
120811	01230	Ody,Kon,MES,Fer	0.31	4.3×10^{-6}	10-10000	1.1×10^{14}	1.9×10^{19}	1.2×10^{17}	4.2×10^{19}	No	9,11,28,29,30,31
121023	27857	Ody,MES,Fer	0.51	7.7×10^{-7}	10-1000	9.2×10^{15}	3.2×10^{19}	3.1×10^{17}	1.0×10^{20}	No	9,11
121127	78960	Ody,Kon,INT,MES	0.53	2.8×10^{-6}	10-10000	5.6×10^{14}	4.1×10^{19}	1.7×10^{17}	5.3×10^{19}	No	11,12,32,33,34
130501	00831	Ody,Kon,MES,Suz	0.41	2.0×10^{-6}	10-10000	7.7×10^{13}	2.0×10^{19}	1.9×10^{17}	6.2×10^{19}	No	13
130504B	27123	Ody,Kon,MES	0.36	8.8×10^{-6}	10-10000	3.2×10^{13}	9.2×10^{18}	8.8×10^{16}	3.0×10^{19}	No	35,36,37,38
131126A	14050	Ody,Kon,MES,Fer	0.12	2.3×10^{-6}	10-10000	3.1×10^{14}	2.0×10^{19}	1.4×10^{17}	5.8×10^{19}	39	40,41,42

Table 2—Continued

GRB	SOD	Spacecraft ^a	Dur., s	Fluence erg cm ⁻²	Energy range, keV	Minimum Distance, cm.	Maximum detectable dist., cm.	Maximum detectable dist., (η _{rD}) ^{0.5} cm. (SEM Model)	Maximum detectable dist., (η _{rD}) ^{0.5} cm. (HM Model)	Counterpart search?	Refs.
140414B	80735	Ody,Kon,INT,MES	0.97	2.3×10^{-6}	10–10000	3.7×10^{14}	2.0×10^{19}	2.0×10^{17}	5.9×10^{19}	No	13
140807	43173	Ody,Kon,MES,Fer	0.57	2.6×10^{-6}	10–10000	1.5×10^{18}	1.8×10^{19}	1.8×10^{17}	5.5×10^{19}	43	13
140906C	85869	Ody,Kon,INT,MES	0.13	2.3×10^{-6}	10–10000	1.3×10^{17}	1.9×10^{19}	1.5×10^{17}	5.8×10^{19}	No	44,45
141011A	24380	Ody,Kon,MES,Fer	0.06	1.4×10^{-6}	10–10000	6.0×10^{13}	2.5×10^{19}	1.6×10^{17}	7.3×10^{19}	No	46,47,48

^aFer: *Fermi*, INT: *International Gamma-Ray Laboratory*, Kon: *Konus-Wind*, MES: *Mercury Surface, Space Environment, Geochemistry, and Ranging* mission, NEAR: *Near Earth Asteroid Rendezvous* mission, Ody: *Mars Odyssey*, Phe: *Phebus*, PVO: *Pioneer Venus Orbiter*, RHE: *Ramaty High Energy Solar Spectroscopic Imager*, SAX: *Satellite per Astronomia X (BeppoSAX)*, Suz: *Suzaku*, Swi: *Swift* (burst was outside the coded field of view of the BAT, and not localized by it), Uly: *Ulysses*

References. — (1) Terekhov et al. (1994); (2) Goldstein et al. (2013); (3) Paciasas et al. (1999); (4) <http://www.ioffe.ru/LEA/shortGRBs/Catalog/>; (5) Pal'shin et al. (2013); (6) <http://ssl.berkeley.edu/ipn3/index.html>; (7) Frontera et al. (2009); (8) <http://www.batse.msfc.nasa.gov/batse/grb/catalog/current>; (9) Goldstein et al. (2012); (10) Paciasas et al. (2012); (11) von Kienlin et al. (2014); (12) Goldstein et al. (2012); (13) Svinikin et al. (2015b); (14) Masetti et al. (2000); (15) Hurley et al. (2002); (16) Park et al. (2000); (17) Price et al. (2000); (18) Vreeswijk and Rol (2000); (19) Guirrec et al. (2010); (20) Golenetskii et al. (2011a); (21) Golenetskii et al. (2011b); (22) Yasuda et al. (2011); (23) Hurley et al. (2011a); (24) Golenetskii et al. (2011c); (25) Golenetskii et al. (2012a); (26) Golenetskii et al. (2012b); (27) Sakamoto et al. (2012); (28) Golenetskii et al. (2012c); (29) Golenetskii et al. (2012d); (30) Golenetskii et al. (2012e); (31) Xiong and Meegan (2012); (32) Golenetskii et al. (2012f); (33) Golenetskii et al. (2012g); (34) Ishida et al. (2012); (35) Vreeswijk and Rol (2000); (36) Golenetskii et al. (2013a); (37) Golenetskii et al. (2013b); (38) Yasuda et al. (2013); (39) Singer et al. (2013c); (40) Golenetskii et al. (2013d); (41) Golenetskii et al. (2013e); (42) Pelassa and Meegan (2013); (43) Singer (2014); (44) Golenetskii et al. (2014a); (45) Golenetskii et al. (2014b); (46) von Kienlin (2014); (47) Golenetskii et al. (2014c); (48) Golenetskii et al. (2014d)

Table 3. Localizations of IPN gamma-ray bursts assuming infinite distances. Some bursts have two possible error boxes; GRB080203 has an eight-cornered error box.

GRB	α	δ
<hr/>		
910206		
Center	87.5650	17.3372
Corners	86.7457	17.8617
	88.4371	16.5674
	86.6713	18.2592
	88.3683	16.9025
OR		
Center	86.9621	36.1678
Corners	86.0419	35.5941
	87.9516	36.9783
	85.9902	35.1926
	87.8875	36.6407
<hr/>		
920414		
Center	90.5234	-76.3115
Corners	90.6025	-76.3287
	90.3189	-76.2150
	90.7309	-76.4079
	90.4446	-76.2943
<hr/>		
970902		
Center	351.0259	+7.3294
Corners	351.0744	+7.3080
	351.1009	+7.3100
	350.9774	+7.3507
	350.9509	+7.3486
<hr/>		
970921		
Center	235.8826	-24.8310
Corners	236.0899	-24.3906
	236.2034	-24.1627
	235.6864	-25.2436
	235.5867	-25.4367
<hr/>		
981102		
Center	277.0514	-48.3354
Corners	277.0532	-48.3258
	277.0159	-48.2744
	277.0496	-48.3449
	277.0870	-48.3962
<hr/>		

Table 3—Continued

GRB	α	δ
990712		
Center	123.4627	+6.6755
Corners	123.8544	+7.2952
	123.2666	+6.3351
	123.2036	+6.2494
	123.7301	+7.1201
OR		
Center	125.3550	+9.4408
Corners	124.9180	+8.8500
	125.6024	+9.7478
	125.6597	+9.8378
	125.0364	+9.0294
000607		
Center	38.4971	+17.1419
Corners	38.4656	+17.1016
	38.5472	+17.2317
	38.5287	+17.1823
	38.4470	+17.0523
001025		
Center	275.3488	-5.1067
Corners	275.4272	-5.1411
	275.1851	-4.9912
	275.2707	-5.0723
	275.5140	-5.2229
001204		
Center	40.2997	+12.8817
Corners	40.2796	+12.8928
	40.3478	+12.8979
	40.3199	+12.8707
	40.2516	+12.8656
010104		
Center	317.3689	+63.5116
Corners	317.6201	+63.5227
	317.5851	+63.4776
	317.1183	+63.5004
	317.1523	+63.5455
010119		
Center	283.4446	+11.9964
Corners	283.4892	+12.0007
	283.4159	+11.9832
	283.4000	+11.9921
	283.4734	+12.0096

Table 3—Continued

GRB	α	δ
<hr/>		
080203		
Center	48.2086	+24.3289
Corners	48.1704	+24.3216
	48.2401	+24.0161
	49.1541	+20.8021
	48.9850	+21.5848
	48.2469	+24.3362
	47.7229	+27.1306
	47.5349	+27.9115
	48.1002	+24.6272
<hr/>		
080222		
Center	68.7192	+56.9390
Corners	69.2723	+57.0738
	68.1039	+56.6937
	68.1686	+56.7979
	69.3407	+57.1754
<hr/>		
080530		
Center	5.3443	28.2246
Corners	5.2701	28.3257
	5.4170	28.1570
	5.2717	28.2920
	5.4186	28.1232
<hr/>		
090228		
Center	98.7014	-28.7863
Corners	98.7827	-28.8531
	98.5307	-28.6112
	98.5698	-28.6709
	98.8219	-28.9123
<hr/>		

Table 3—Continued

GRB	α	δ
090523		
Center	22.8383	-62.2047
Corners	23.0738	-62.1859
	23.2792	-62.2169
	22.6023	-62.2230
	22.3971	-62.1907
100223		
Center	101.6711	+12.8302
Corners	101.9024	+12.6261
	101.4091	+13.4941
	101.5176	+12.9034
	102.0085	+12.0774
100629		
Center	227.6190	+29.5479
Corners	227.6295	+29.2934
	227.5705	+29.7415
	227.6081	+29.8012
	227.6671	+29.3536
100811		
Center	344.9605	+20.6223
Corners	344.9395	+20.5411
	345.0289	+20.6525
	344.9816	+20.7032
	344.8922	+20.5919
101009		
Center	75.6068	-33.9325
Corners	75.8367	-33.8146
	76.0209	-33.6624
	75.1904	-34.1986
	75.3765	-34.0492
101129		
Center	268.6211	-7.7232
Corners	272.2014	-9.1377
	265.1168	-6.9176
	272.2546	-9.3668
	265.1792	-7.0998
110510		
Center	336.1407	-44.0726
Corners	344.4202	-52.3621
	344.5801	-52.3041
	327.7177	-35.8320
	327.8448	-35.7920

Table 3—Continued

GRB	α	δ
110705		
Center	156.0322	40.1169
Corners	156.1434	40.1805
	156.0390	39.9001
	156.0246	40.3325
	155.9211	40.0532
110802		
Center	44.4655	33.0037
Corners	44.4647	33.6264
	44.4285	32.4871
	44.5087	33.5009
	44.4754	32.3503
120222		
Center	296.9268	14.7102
Corners	290.7915	-5.6861
	291.1995	-2.6858
	304.9807	31.3395
	307.1167	33.7741
120519		
Center	178.0457	21.9477
Corners	178.2141	22.2660
	178.2885	22.1813
	177.8043	21.7128
	177.8781	21.6273
120811		
Center	43.7599	-31.9123
Corners	43.8831	-31.9728
	43.7269	-32.0579
	43.7928	-31.7664
	43.6370	-31.8516
121023		
Center	313.3540	-4.6025
Corners	315.3258	-8.9120
	311.5238	-0.2314
	315.1761	-8.9571
	311.3903	-0.3093
121127		
Center	176.4314	-52.4316
Corners	176.2965	-52.4618
	176.4549	-52.2522
	176.4080	-52.6106
	176.5661	-52.4011

Table 3—Continued

GRB	α	δ
130501		
Center	350.5102	16.7266
Corners	350.4295	16.8223
	350.4890	15.7404
	350.5512	17.6829
	350.5910	16.6309
130504B		
Center	347.1594	-3.8325
Corners	347.0950	-3.8347
	349.6913	-9.6653
	345.9151	-0.2257
	347.2238	-3.8303
131126A		
Center	202.8995	51.5581
Corners	202.9690	51.6343
	203.1321	51.5592
	202.6668	51.5564
	202.8303	51.4819
140414B		
Center	121.8042	-38.1211
Corners	121.2343	-35.5319
	121.0519	-33.7849
	122.7335	-42.2323
	122.4453	-40.6251
140807		
Center	188.8547	36.2259
Corners	188.9062	36.3820
	188.7683	36.3184
	188.9406	36.1333
	188.8030	36.0695
140906C		
Center	314.9144	2.0606
Corners	314.8105	2.5705
	314.9946	2.0906
	314.8341	2.0305
	315.0226	1.5373
141011A		
Center	257.9473	-9.6520
Corners	258.0072	-9.3553
	257.7749	-9.3571
	258.1189	-9.9487
	257.8862	-9.9489